THE PENNSYLVANIA STATE UNIVERSITY
SCHREYER HONORS COLLEGE

DEPARTMENT OF CHEMISTRY

Core-Sheath Nanofiber Composites with Shape Memory Properties

ASNA RIZWAN
SPRING 2023

A thesis
submitted in partial fulfillment
of the requirements
for a baccalaureate degree
in Chemistry
with honors in Chemistry

Reviewed and approved* by the following:

Patrick T. Mather
Dean of Schreyer Honors College
Professor Chemical Engineering
Thesis Supervisor

Elizabeth Elacqua
Assistant Professor of Chemistry
Honors Adviser

* Electronic approvals are on file.

ABSTRACT

Shape Memory Polymers (SMPs) are a class of smart materials with the ability to recover its original shape from deformation following exposure to an external stimuli such as heat or light. SMPs exhibit a wide range of applications in biomedical devices, sensors, actuators, smart textiles, and aerospace components. Polymer composites with shape memory properties have been fabricated using electrospinning techniques that allow for efficient production and precise control over fiber properties. This study utilizes electrospinning-based research to produce novel core-sheath poly(ε-caprolactone) (PCL) (sheath) and Pellethane (core) fibers that demonstrate shape memory behavior and reversible adhesive properties. Further research is needed to investigate balancing delicate electrospinning conditions for improved control over core-sheath fiber production.

TABLE OF CONTENTS

LIST OF FIGURES

LIST OF TABLES

ACKNOWLEDGEMENTS

A special thanks to Dean Mather for his continued support, guidance, and patience throughout this process. From his mentorship, I have learned so much about myself as a student, a researcher and as a person, and I cannot thank him enough for the valuable skills I've acquired and (mostly difficult) lessons I've learned over the past year.

I would also like to thank my peers in the Mather Research Group for all their help over the summer and throughout the academic year with training, advice, and any sort of assistance in the lab when needed!

Chapter 1

Introduction & Background

1.1 Shape Memory Polymers

Shape Memory Polymers (SMPs) are a class of smart materials that are able to "memorize" its original state after deformation to a fixed, temporary state. Triggered by an external stimulus such as heat or light, these materials are capable of undergoing a reversible phase transition from a temporary shape to a permanent shape and back again[1].

SMPs have a wide range of potential applications, including biomedical devices, aerospace materials, textiles, and smart packaging. SMPs could be used to create self-fitting medical implants or shape-changing drug delivery systems and have potential in further advancements of self-healing materials.

SMPs usually contain two components: a "fixing" and a "memory" component[2]. When the SMP is heated above its glass transition temperature, it becomes soft and can be easily deformed into a new shape. The SMP, when cooled below its glass transition temperature, becomes stiff and retains its new shape. Completing the loop, subsequent heating returns the material to its original, stress-free shape.

1.2 Developments in Shape Memory Polymers

Buffington et. al[3] reported biologically-responsive shape memory polymers with a shape-fixing component poly(ε-caprolactone) (PCL) and a shape memory component Pellethane. SMPs were designed using dual electrospinning, and the cytocompatible materials responded directly to enzymatic activity[4]. Other studies have designed polymer blends of thermoplastic polyurethane (TPU) elastomers with a

thermoplastic healing agent PCL with demonstrated self-healing and shape memory properties. This thesis expands upon this work by utilizing PCL and Pellethane to electrospin materials in a different arrangement.

1.3 Material Selection

Pellethane® is a family of medical-grade, thermoplastic polyurethanes (TPUs) known for their and wide range of hardness. A versatile elastomer, Pellethane® exhibits characteristics of both plastics and rubber. Pellethane® is a linear block copolymer consisting of hard and soft segments: the hard segments are isocyanates (aliphatic or aromatic) and the soft segments are made of reacted polyol[1]. This study uses Pellethane® 5863-80A ("Pellethane"), an aromatic polyether TPU. At a softer grade, Pellethane is considered nearly amorphous with no definite melting point, softening gradually with exposure to heat.

Poly (ε-caprolactone) (PCL) is a biodegradable, semi-crystalline thermoplastic polyester with mechanical properties such as flexibility, toughness, and resistance to fatigue. PCL has a low melting point of around -60 ℃ and a glass transition temperature of approximately -60 ℃. PCL's low melting point and material lifetime provide utility in the development of artificial implants and for use in tissue engineering. Furthermore, various drugs have been incorporated into PCL beads for controlled-release drug delivery systems.

Biodegradability, biocompatibility, compatibility with other polymers, low cost and processibility of these compounds make them excellent candidates for shape memory materials.

1.4 Coaxial Electrospinning

Electrospinning is a versatile and efficient fiber-production method that enables control over various fiber properties, producing nano- and microscale fibers with a high surface area to volume ratio and high porosity. The advantages offered by the technique allow for scaling-up the production of fibers for commercial use.

For a conventional, uniaxial electrospinning apparatus, an electrostatic force forms a charged jet of polymer solution extruded through a metallic needle connected to a high voltage power supply. The polymer is elongated into fibers as it deposits onto a grounded (or otherwise oppositely charged) metal drum. A characteristic “Taylor cone jet” is formed during this process: a conical-shaped droplet that emerges from the spinneret due to overcome surface tension.

However, this technique was modified to allow for the production of polymer composites, particularly in a coaxial arrangement in which one polymer occupies the core and another polymer forms the sheath layer[2]. The coaxial electrospinning apparatus is shown in Figure 1-1. Two compatible polymer solutions are simultaneously fed into a coaxial spinneret, an inner needle containing core fluid while a solution from the outer needle encloses the core to form the sheath.

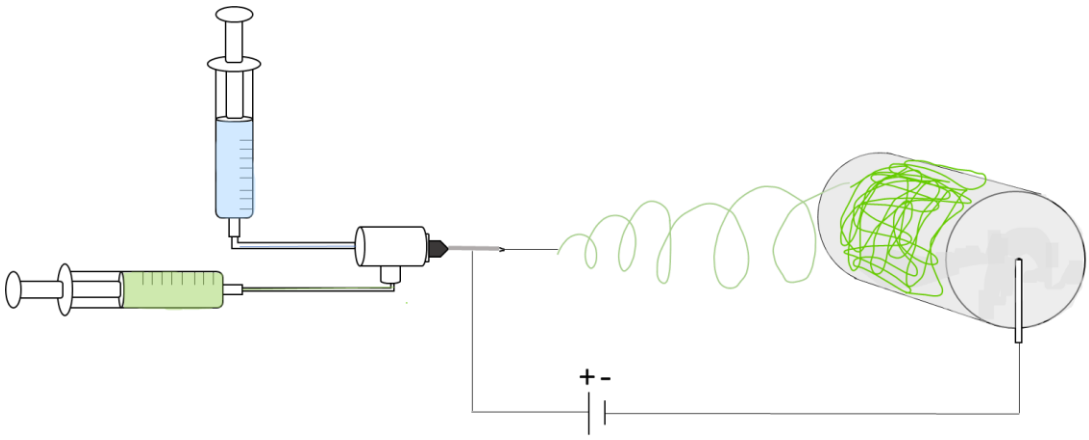

Figure 1-1: Coaxial electrospinning setup with inner (blue) and outer (green) polymer solutions feeding through coaxial spinneret. Charged fluid from an applied voltage forms jet that deposits on rotating metal drum.

A review by Moghe and Gupta[3] discusses several considerations regarding material preparation and electrospinning parameters for the production of core-sheath fibers. Maintaining stability of the Taylor cone jet enables coaxial electrospinning (Figure 1-2), and thus, the interactions between the core-sheath solutions must be taken into account, during both the selection of materials and processing parameters (applied voltage, flow rate, etc.).

1. *Solution Viscosity*: The viscosity of the sheath solution is shown to be more critical to the success of core-sheath structure formation than the core fluid. The viscous stress imparted on the core by the sheath fluid must be sufficient to overcome the interfacial tension between the two solutions.
2. *Solvent/Solution Miscibility*: Materials should be selected to prevent precipitation of the other polymer from solution when both solutions meet at the tip of the spinneret. Additionally, the interfacial tension between the core and sheath solution should be minimized to form a stable Taylor cone.
3. *Applied Voltage*: Studying Gelatin/PCL (sheath/core) polymer systems, Moghe and Gupta describe a critical voltage range that enables Taylor cone stability, a range as

small as 1 kV. Applying a higher or lower voltage than the prescribed range will not result in optimum spinning.

4. *Solution Flow Rates*: The core flow rate should generally be lower than that of the sheath to prevent mixing of inner and outer fluids. However, using a low core flow rate may result in insufficient incorporation of the core into the fiber. Several polymer systems previously studied utilized a 3:1 core-sheath flow rate ratio.

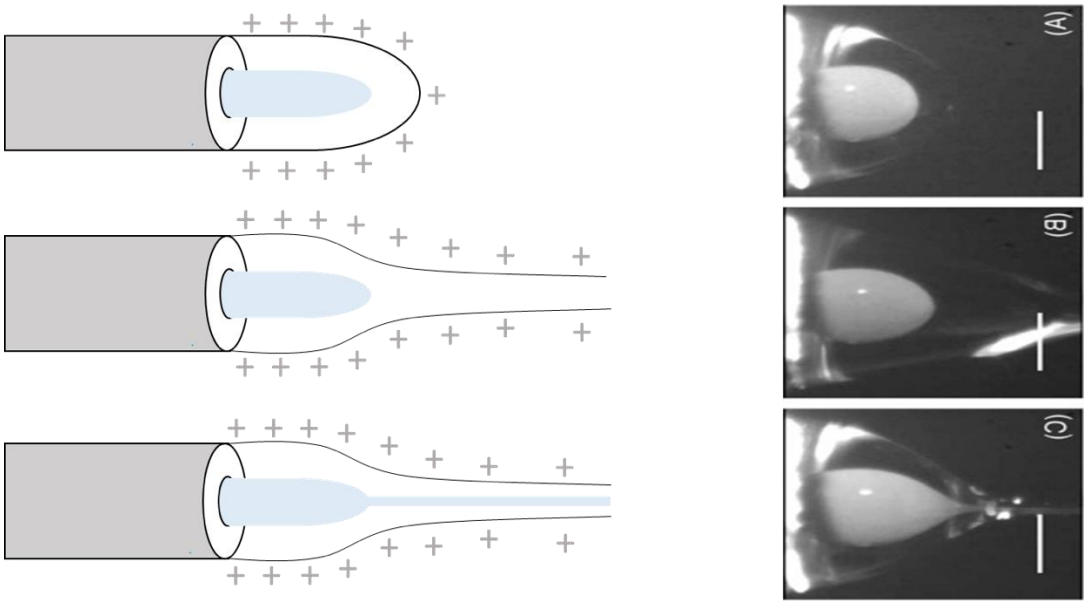

Figure 1-2: Progression of charged jet under electric field for coaxial electrospinning by gradual increase in voltage for (vinyl pyrrolidone) (PVP, outer) and a mineral oil (inner) solutions, resulting in formation of stable Taylor cone.

Chapter 2

Fabrication and Characterization of Core-Sheath Fibers

2.1 Materials

Polycaprolactone (PCL), chloroform, tetrahydrofuran, and N,N-Dimethylformamide were purchased from Sigma Aldrich. Pellethane® 5863-80A was obtained from Lubrizol Corporation.

2.2 Coaxial Electrospinning

Solutions of 13 w/v% Pellethane in a 3:2 THF:DMF solvent mixture and 18 w/v% PCL in 4:1 chloroform:DMF solvent mixture were prepared prior to electrospinning. Polymer solutions were transferred to separate syringes and injected through 1 mm diameter Teflon tubing. Syringes containing Pellethane and PCL solutions were attached to a coaxial needle such that 13 w/v% Pellethane would flow through the inner needle surrounded by a flow of 18 w/v% PCL in an outer concentric needle. All electrospinning was performed with a 20 cm needle-to-collector distance, speed of 1500 rpm for the metal drum, and -1 kV charge at the collector. A rotating metal drum (collector) was wrapped in foil, and a thin layer of Pol-Ease® release agent was applied to the surface to easily remove the electrospun web from the drum.

Two series of core-sheath PEL-PCL fibers were fabricated. The first series increases the weight percent of Pellethane by 10% and 25% by adjusting the flow rates of both PCL and PEL while holding the total mass flow rate constant (Table 2-1). The second series of core-sheath webs holds the mass flow rate (and flow rate) of PEL constant and changes the weight percent of Pellethane by decreasing the flow rate of PCL (Table 2-2). The tables below summarize the

parameters for each electrospun core-sheath fiber: the solution flow rate of PCL (Q_{PCL}), flow rate of Pellethane (Q_{PEL}) and applied voltage at needle V in kV. The mass flow rate of PCL, $\dot{m}_{PCL}$, and $\dot{m}_{PEL}$, the mass flow rate of Pellethane – calculated from the concentration of the polymer solution and the flow rate – and the theoretical weight percent of PCL expected for each core-sheath web are also listed (Eq. 2.1).

$$w\%_{PCL\ (theor.)} = \frac{\dot{m}_{PCL}}{\dot{m}_{PCL}+\dot{m}_{PEL}} * 100 \qquad (2.1)$$

Table 2-1: Core-Sheath PCL/PEL electrospinning parameters with constant total mass flow rate (ṁ total) and expected percent composition of PCL by weight.

Sample	Q_{PCL} (mL/hr)	Q_{PEL} (mL/hr)	$\dot{m}_{PCL}$ (g/hr)	$\dot{m}_{PEL}$ (g/hr)	$\dot{m}_{Total}$ (g/hr)	$w\%_{PCL(theor.)}$	$+V$ (kV)
1	6.0	2.0	1.08	0.26	1.34	80.6	10.6
2	5.8	2.3	1.05	0.295	1.34	78.1	10.6
3	5.6	2.6	1.005	0.335	1.34	75.0	11.2

Table 2-2: Core-Sheath PCL/PEL electrospinning parameters with constant Pellethane flow rate and expected percent composition of PCL by weight.

Sample	Q_{PCL} (mL/hr)	Q_{PEL} (mL/hr)	$\dot{m}_{PCL}$ (g/hr)	$\dot{m}_{PEL}$ (g/hr)	$\dot{m}_{Total}$ (g/hr)	$w\%_{PCL\ (theor.)}$	$+V$ (kV)
1	6.0	2.0	1.08	0.26	1.34	80.6	10.6
4*	5.3	2.0	1.05	0.26	1.22	78.7	14.4
5*	4.5	2.0	1.005	0.26	1.07	75.7	14.5

*Samples denoted by an asterisk indicate constant Pellethane flow rate and core size

Neat Pellethane and PCL samples were also electrospun using the flow rates from Sample 1 and the enthalpy of melting for PCL was measured (Table 2-3).

Table 2-3: Electrospinning parameters for neat PCL 18 w/v% and neat Pellethane 13 w/v%

Sample	C (g/mL)	Q (mL/hr)	$\dot{m}$ (g/hr)	$+V$ (kV)
PEL	0.13	2.0	1.08	9.0
PCL	0.18	6.0	1.05	14.4

2.3 Differential Scanning Calorimetry

Differential Scanning Calorimetry (DSC), using the DSC Q2000 (TA Instruments), provided a thermal profile for all core-sheath fibers, neat Pellethane, and neat PCL to investigate the melting behavior, glass-rubber transition, and the composition of each sample. Samples (4-5 mg) were first heated to 200 ℃ to erase thermal history, cooled to -50 ℃, and heated to 200 ℃ at a heating/cooling rate of 10 ℃/min. The second heating cycle was evaluated for enthalpy of melting at T_m for PCL and for the glass transitions T_g of Pellethane. The weight percent of PCL was determined from the fraction of the heat of the melting curve for core-sheath composites to the heat of melting of neat PCL (Eq. 2.2). A representative DSC curve of the PCL/PEL core-sheath composites is shown below (Figure 2-1).

$$w\%_{PCL} = \frac{\Delta H_{m,\ PCL-PEL}}{\Delta H_{m,\ PCL}} * 100\% \qquad (2.2)$$

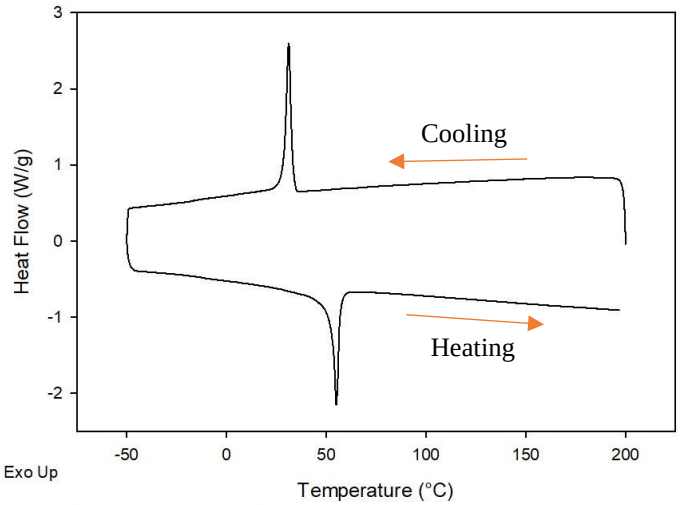

Figure 2-1: Representative DSC second heating curve for PCL/PEL composites (77% PCL).

2.4 Water Contact Angle

A qualitative determination of the wettability of the core-sheath webs and a comparison to that of neat PCL and Pellethane webs indicated which polymer formed the sheath material (indicative of successful coaxial electrospinning). A drop of water was cast on the surface of the fibers, and the hydrophobicity/hydrophilicity of the material was characterized.

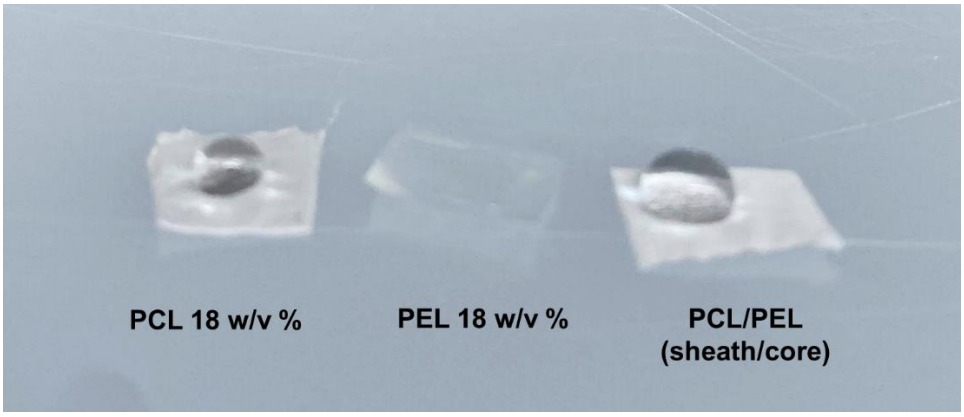

Figure 2-2: Qualitative water contact analysis of neat PCL, neat PEL and PCL/PEL core-sheath webs. Water droplets on PCL and PCL/PEL composite retained its surface tension.

2.5 Scanning Electron Microscopy (SEM)

For visualization of the coaxial structure and surface morphology, Field Emission Scanning Electron Microscopy (FESEM) on the Verios G4 was used. Cross-sections of the core-sheath fibers and the surface (pre- and post-shape memory) were both examined.

For cross-section viewing, cryofacturing the sample was necessary prior to microscopy. Slits were created on each side of a rectangular strip, as shown in Figure 2-2, to facilitate tear propagation. Samples were then cooled in the DMA Q800 (TA Instruments) to -100 ℃ and held for ten minutes before ramping the stress to approximately 15 MPa at a rate of 3 MPa/min until samples were fractured in a brittle manner.

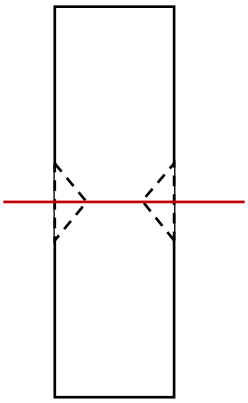

Figure 2-3: Incisions on the dotted line of PCL/PEL samples were made prior to cryofacturing in the DMA.

Samples were sputter coated with 5 nm of iridium due to beam-sensitivity to prevent damage to the sample's morphology. Fibers (cross-sections and surfaces) were viewed using an accelerating voltage of 3.0 kV at 0.10 nA with a typical working distance between 3.0-5.0 mm.

Employing ImageJ and Verios software tools, individual fiber diameters were obtained from SEM images of the surface.

2.6 Dynamic Mechanical Analysis (DMA)

Moduli determination for the materials were performed using the Discovery DMA 850 (TA Instruments). A slender, rectangular strip was annealed in the DMA at 80 ℃ (above PCL's T_m) and held isothermal for 10 minutes. Samples were then cooled to -75 ℃ prior to ramping the temperature to 100 ℃ at a rate of 3 ℃/min. A preload force of 0.01 N, 80μm amplitude, and a force track of 108% were used. From the temperature ramp profile, the glass transition and temperatures were collected in addition to storage modulus at room temperature (20 ℃). An example of a DMA temperature sweep is shown in Figure 2-4 for 72% PCL:PEL, revealing multiple thermal transition accompanying storage and loss modulus changes.

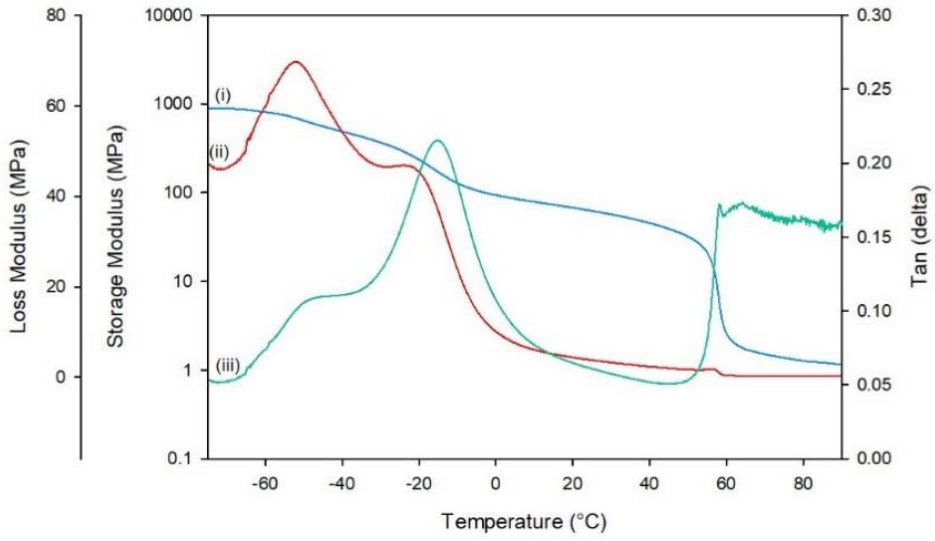

Figure 2-4: Representative DMA curves (i) storage modulus, (ii) loss modulus (iii) tan delta from temperature ramp of 72% PCL. Storage modulus is in log scale.

2.7 Shape Memory Testing

To assess shape memory behavior, core-sheath fibers of varying PCL content were heated, deformed, cooled, and heated again in a prescribed manner using the Discovery DMA 850. Samples were first stretched at 80 ℃ by ramping the stress to 0.35 MPa (0.1 MPa/min) then cooled at 3.0 ℃/min and held isothermally for 10 minutes at -10 ℃ to fix the temporary state. After releasing the stress back to the preload force 0.1 MPa (0.1 MPa/min), samples were heated to 80 ℃ (3 ℃/min) and held isothermal for 10 minutes for shape recovery (Figure 2-5). Repeating the cycle, a three-cycle shape memory program was tested for each core-sheath sample, and the shape fixity (R_f) and recovery (R_r) were calculated for each cycle:

$$R_f(\%) = \frac{\varepsilon_f - \varepsilon_i}{\varepsilon_d - \varepsilon_i} * 100\%$$

$$R_r(\%) = \frac{\varepsilon_f - \varepsilon_r}{\varepsilon_f - \varepsilon_i} * 100\%$$

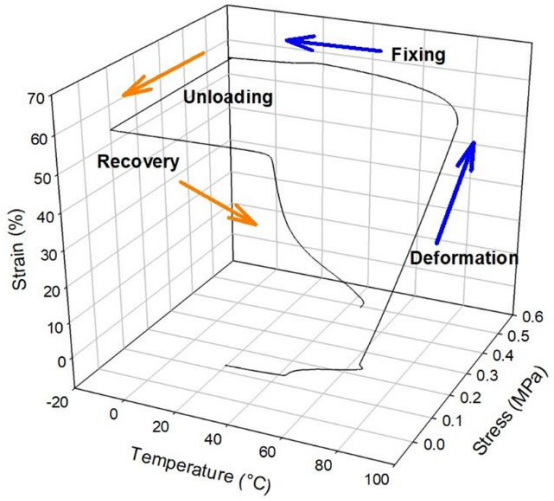

Figure 2-5: Shape Memory program cycle with labeled steps - deformation, fixing, unloading, recovery.

2.8 Mechanical Testing

A CellScale Biomaterials Tensile Tester with 50 N load cell was used to determine the tensile properties of the core-sheath webs. Samples cut into dogbones (ASTM D638-Type 4.25) were stretched at a rate of 0.833 mm/s up until fracture for stress and strain at break. From the linear elastic region, Young's modulus was obtained from the slope of the tangent line. An example stress-strain curve generated for 79% PCL:PEL core-sheath fibers in Figure 2-6 depicts the elastic region from which Young's modulus was obtained and the point of fracture for the material.

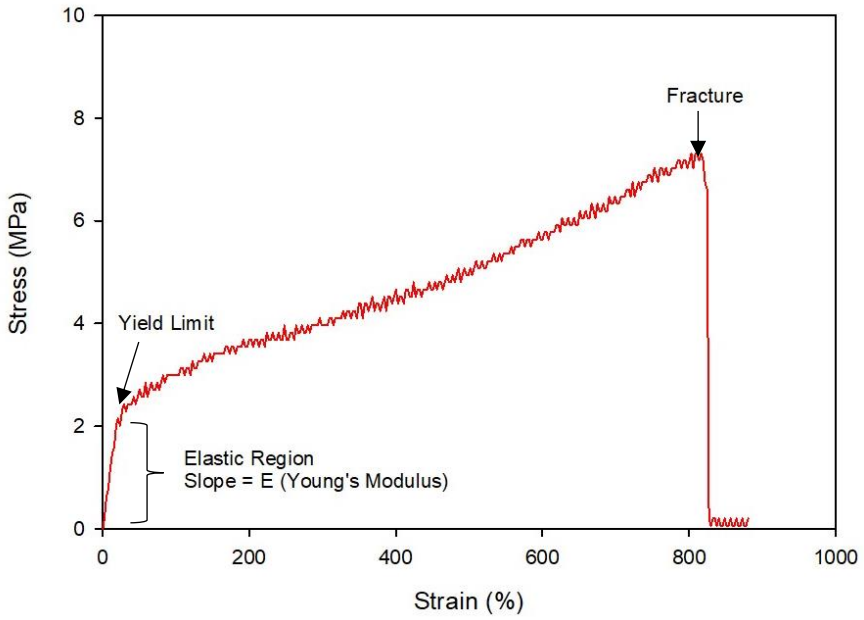

Figure 2-6: Example of stress-strain curve obtained from tensile testing for 79% PCL:PEL* core-sheath fibers.

Chapter 3

Results & Discussion

3.1 Fabrication & Morphology

Visualization of the core-sheath structure and surface morphology for PCL/PEL composites and pure PCL and PEL were studied using SEM. Figure 3-1 shows the surface fibers of neat PCL and

Pellethane. The surface of PCL contained more uniformity among fibers whereas Pellethane fibers appeared melded together with small, interspersed fibers throughout the surface.

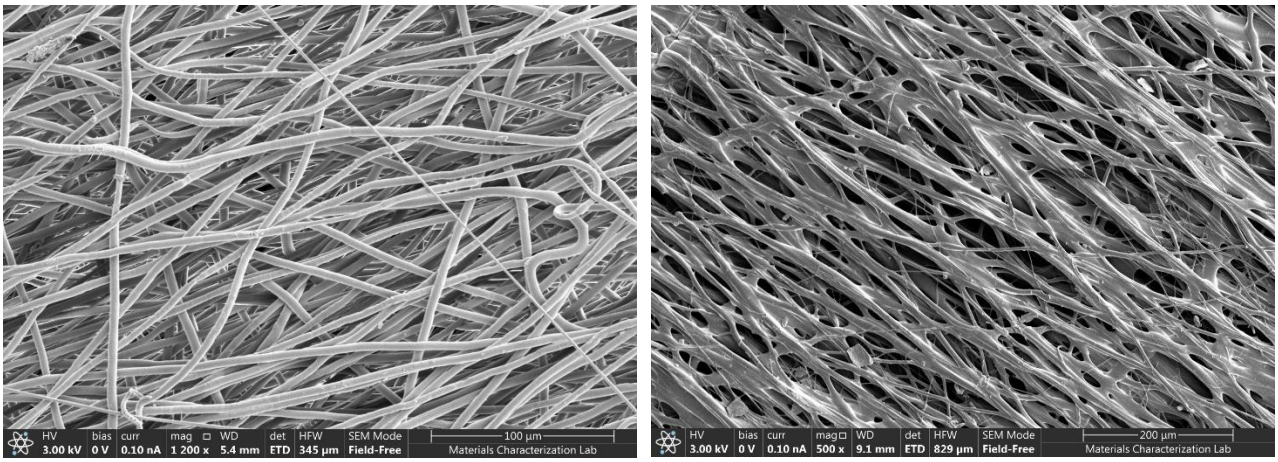

Figure 3-1: SEM images of neat PCL (left) and neat Pellethane (right).

The coaxial arrangement of PCL and Pellethane was located among individual fibers in a cross-section of the sample. Despite the visual similarity of both polymers in SEM images, an outline of the core surrounded by a layer of polymer (sheath) in the coaxial fibers was distinguishable. Figure 3-2 shows the cross-section of a fiber with visible core-sheath arrangement. Within all PCL/PEL composites, the core was not directly centered in the fiber as the inner nozzle was not directly centered in the coaxial spinneret prior to electrospinning. Furthermore, while the images do not contain any notable features that assist in determining the specific polymer that occupies the core or the sheath, the sheath fibers from surface images somewhat resemble that of neat PCL.

Figure 3-3 and Figure 3-4 depict side-by-side images of the surface morphology and the core-sheath structure for each PCL/PEL composite.

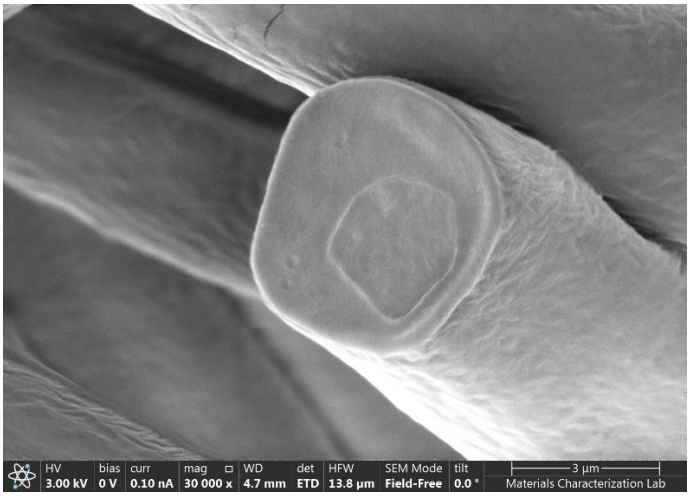

Figure 3-2: SEM visualization of core surrounded by sheath polymer in PCL/PEL fiber cross-sections at 30,000x magnification.

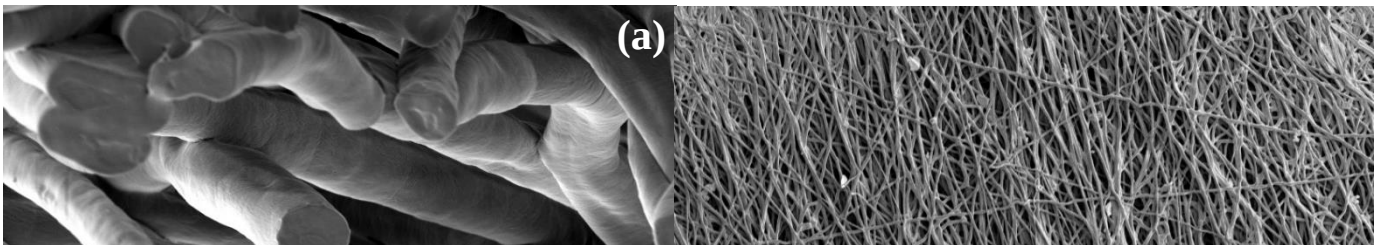

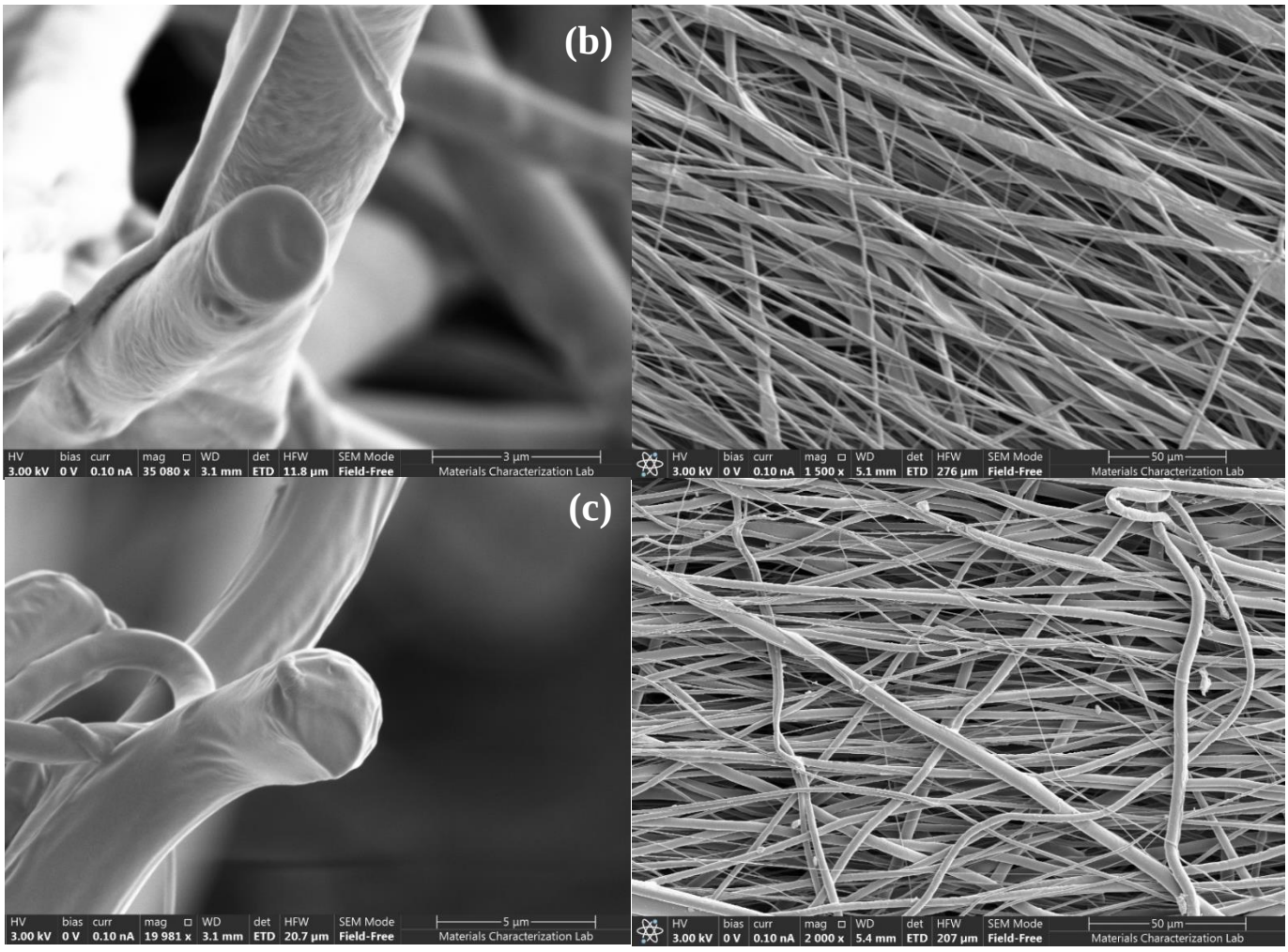

Figure 3-3: SEM images of coaxial fiber cross-section (left) and surface morphology (right) for (a) 45% PCL, (b) 74%, and (c) 72% PCL:PEL composites.

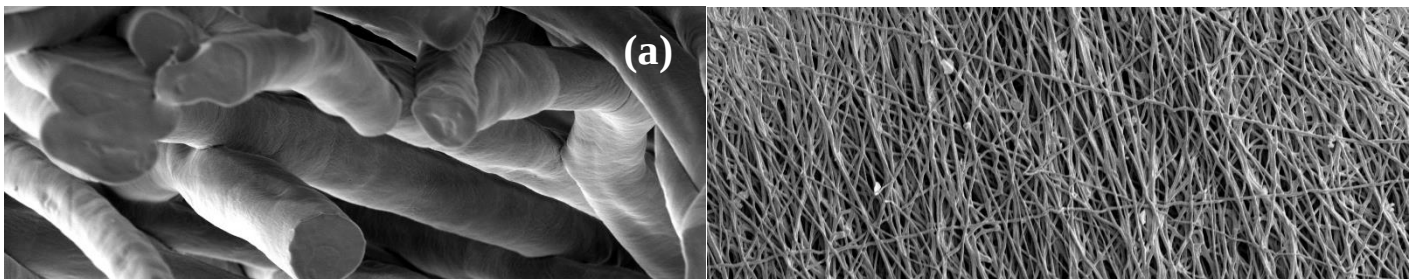

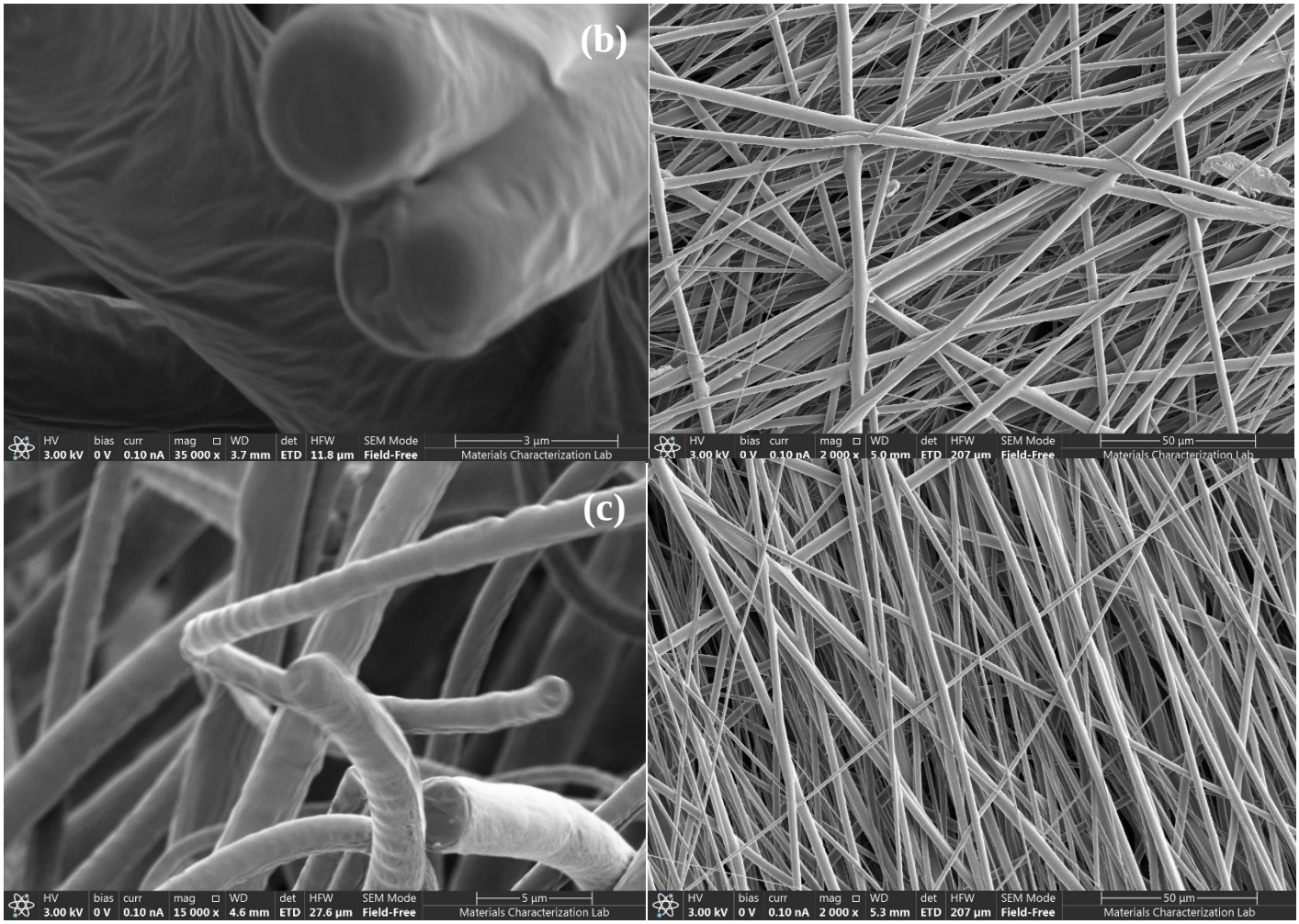

Figure 3-4: SEM images of coaxial fiber cross-section (left) and surface morphology (right) for (a) 45% PCL, (b) 79%, and (c) 77% PCL:PEL* composites.

for a distribution of fibers, and the average fiber diameters for core-sheath PCL/PEL composites neat PCL and PEL were recorded on a microfiber scale in Table 3-1. A comparison of the distribution of fiber

diameters of PCL/PEL core-sheath webs for samples with constant total mass flow rate, constant PEL flow rate (Figure 3-5), and core-sheath fiber diameters to neat PCL and PEL (Figure 3-6) are shown on a nanometer scale. The distributions of all samples reflect unimodality. The average fiber diameter of 45% PCL (Sample 1) core-sheath fibers was more than double the other PCL/PEL composites, which were within the 1.4 – 2.2 µm range. Generally, PCL/PEL composite fibers were smaller in diameter than pure PCL and PEL fibers. Furthermore, 45% PCL/PEL and neat Pellethane fibers contained a larger distribution of diameter lengths than other webs.

Table 3-1: Average fiber diameters (µm) of core-sheath PCL:PEL composites with varying PCL content and controls obtained from Image J software.

Sample	$w\%_{PCL\,(obs.)}$	Fiber Diameter (µm)
1	45	5.82 ± 1.50
2	74	1.66 ± 1.04
3	72	1.38 ± 1.02
4*	79	2.14 ± 1.04
5*	77	1.99 ± 0.96
pure PCL		4.27 ± 0.74
pure PEL		4.43 ± 2.93

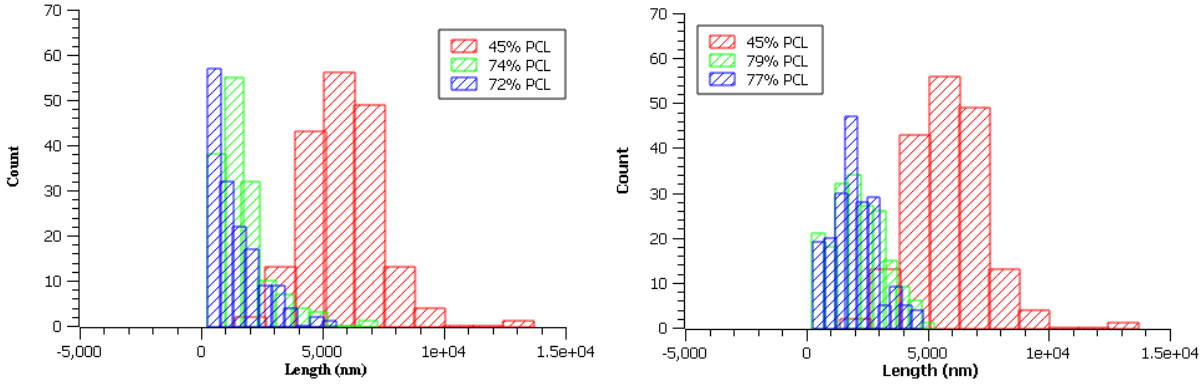

Figure 3-5: Histograms of core-sheath PCL:PEL fiber diameters (nm) with varying PCL content. Fibers were electrospun with constant total mass flow rate (left) and constant PEL flow rate (right).

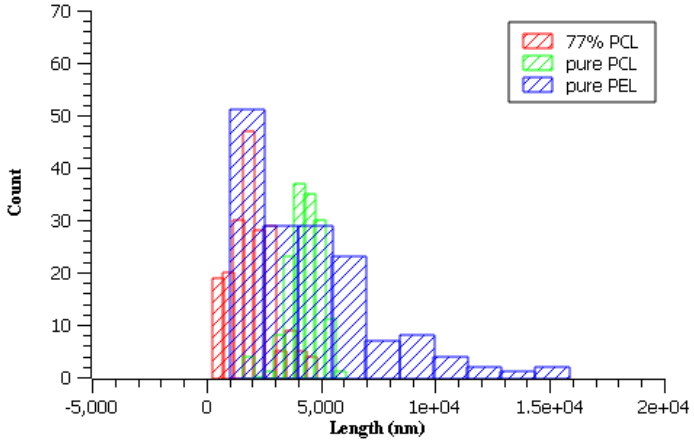

Figure 3-6: Histograms of pure PCL and PEL fiber diameters (nm) compared to 77% PCL:PEL core-sheath composites

3.2 Thermal Characterization

Using second DSC heating curves, transition temperatures of the PCL/PEL composites, neat PCL and neat Pellethane webs were obtained. Shown in Figure 3-7, the melting transition temperatures for the core-sheath webs were nearly identical to neat PCL at 55 ℃ (Figure 3-8). In Figure 3-9, the glass transition temperature of neat Pellethane was observed at T_g = -12.3 ℃, but the transition was difficult to detect among the PCL:PEL samples from DSC. The literature glass transition temperature of Pellethane is -37 ℃.

Enthalpy (J/g) differed for each composite as a result of the difference in relative composition of PCL:PEL. An increase in the percent composition of Pellethane resulted in a lower heat of melting relative to neat PCL. Approximations of the weight percentage of PCL for core-sheath composites were calculated from the heat of melting at PCL's T_m.

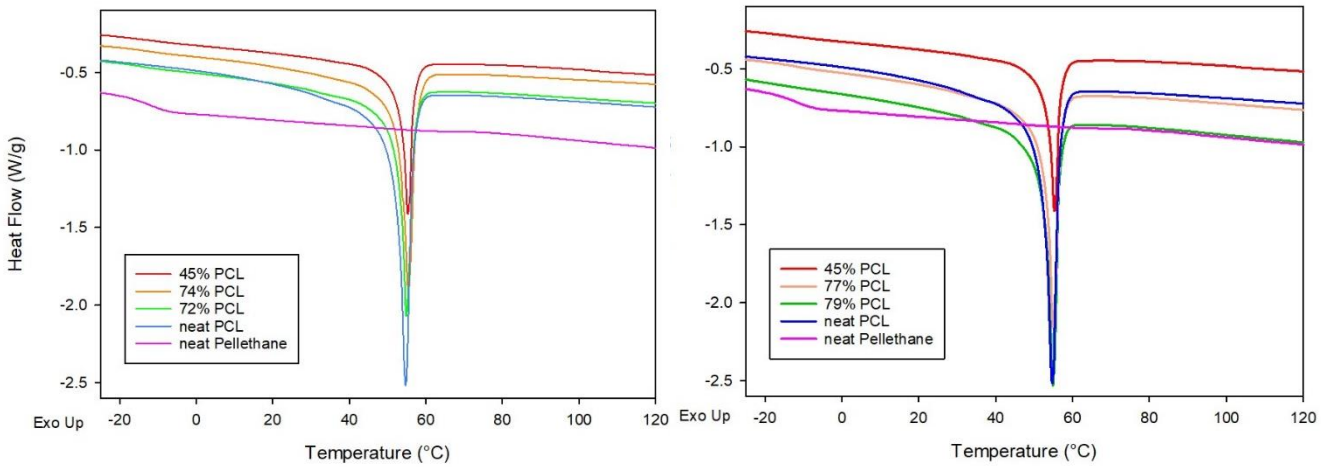

Figure 3-7: DSC second heating melting curves of PCL:PEL composites of varying relative %PCL composition for samples prepared with const. total ṁ samples (left) and const. PEL flow rate (right).

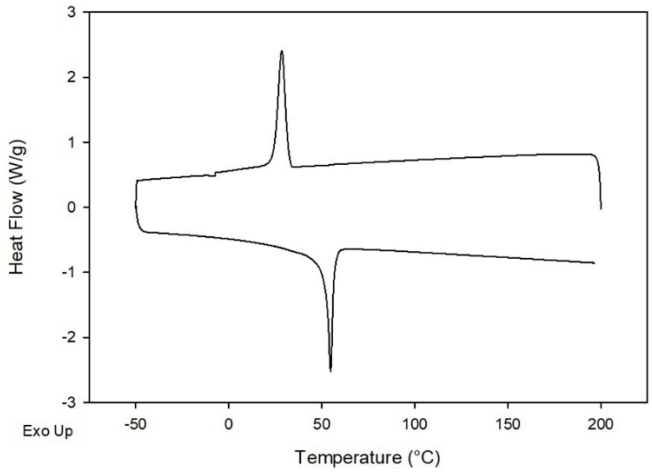

Figure 3-8: DSC second heating curve (erased thermal history) of neat PCL with cooling (29 °C) and melting (55 °C) curves.

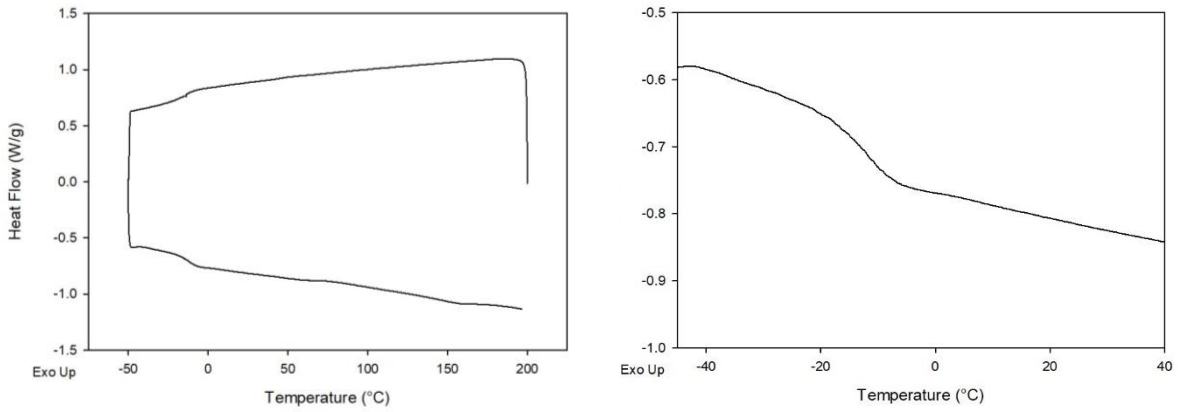

Figure 3-9: DSC second heating curves of neat PCL with glass transition Tg at -12.3 ℃ from the midpoint. Measurement on the right shows zoomed-in region of transition.

Table 3-2 summarizes the heat of melting, the observed weight percentage of PCL and the estimated PCL composition calculated from electrospinning parameters. Four of the core-sheath PCL:PEL composites (Samples 2-5) were within the range of 70-80% PCL composition while DSC showed the first sample contained 45% PCL:PEL, much lower than predicted.

Table 3-2: Enthalpy of melting (J/g) observed for core-sheath PCL:PEL composites. Ratio of observed enthalpy to enthalpy of melting of neat PCL was compared to predicted composition from electrospinning parameters.

Sample	ΔH_m **PCL (J/g)**	$w\%_{PCL\ (obs.)}$	$w\%_{PCL\ (theor.)}$
1	29.62	45.4	80.6
2	48.53	74.4	78.1
3	47.25	72.4	75.0
4	51.55	79	78.7
5	50.24	77	75.7

3.3 Mechanical Characterization

DMA was also used to determine the transition temperatures of the PCL:PEL core-sheath webs at the glass transition and melting of PCL and Pellethane. Given the DMA's sensitivity in monitoring mechanical changes to an increase in temperature, the glass transition of Pellethane (T_g = -26.02 ± 0.40 ℃) for the core-sheath samples was more easily visualized in the DMA compared to DSC. Figure 3-10 shows storage modulus (E'), loss modulus (E") and tan delta as a function of temperature for neat PCL and Pellethane obtained from the peak in the loss modulus curve.

For PCL:PEL composites, DMA curves of the samples exhibited high storage modulus at lower temperatures (attributed to Pellethane). Figure 3-11 depicts the storage modulus of all core-sheath fibers between -75 to 70 ℃. At lower temperatures, storage modulus generally decreases with increasing PCL composition, but this trend was not applicable at room temperature. Individual representative DMA curves of the core-sheath composites are also shown in Figures 3-12 to 3-16 which show the presence of a rubbery plateau region at temperatures higher than PCL's T_m, indicating shape memory potential. Table 3-3 summarizes the glass transition temperatures of PCL and PEL obtained from tan delta peaks and storage modulus at ambient temperatures (20 ℃). Glass transition temperatures for core-sheath composites were more than 2 degrees higher than T_g observed for neat Pellethane and slightly

lower than T_g for neat PCL. All samples except for 74% PCL:PEL exhibited a higher room temperature storage modulus than the controls.

Table 3-3: Glass transition temperatures of PEL and PCL and rt E' of core-sheath PCL:PEL composites obtained from DMA temperature ramp

Sample	T_g PEL (℃)	T_g PCL (℃)	RT E' (MPa)
45% PCL:PEL	-23.09 ± 1.78	-56.29 ± 1.96	67.67 ± 2.80
72% PCL:PEL	-23.02 ± 1.55	-52.39 ± 0.66	72.43 ± 5.69
74% PCL:PEL	-24.66 ± 0.74	-55.93 ± 2.41	33.44 ± 3.04
77% PCL:PEL*	-21.82 ± 2.72	-55.56 ± 1.46	84.92 ± 14.40
79% PCL:PEL*	-20.95	-52.48	50.34
pure PCL	-	-53.73	59.77
pure PEL	-26.02 ± 0.40	-	8.95 ± 0.01

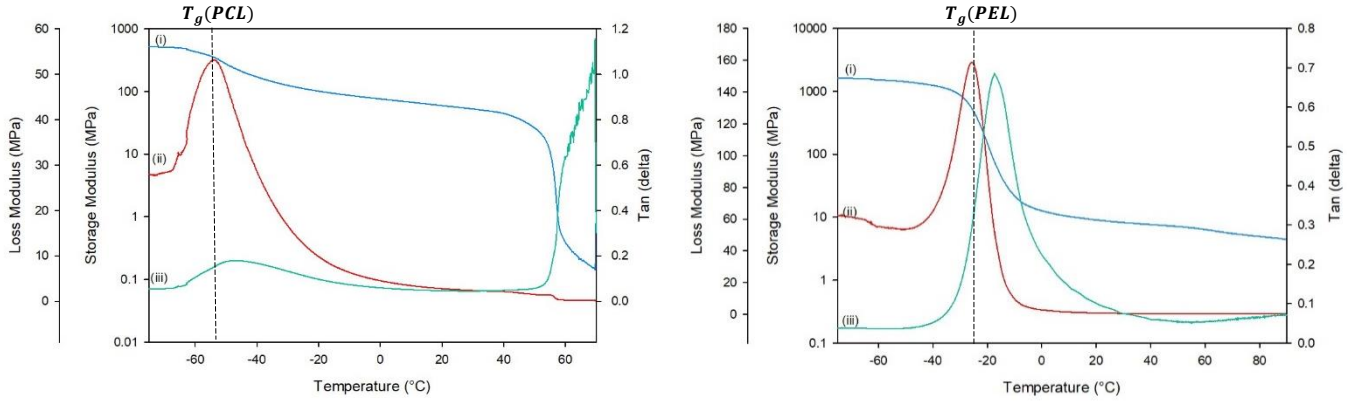

Figure 3-10: Representative DMA curves for neat PCL (left) and neat Pellethane (right) from -75 to 90 ℃. Storage modulus is shown in a logarithmic scale.

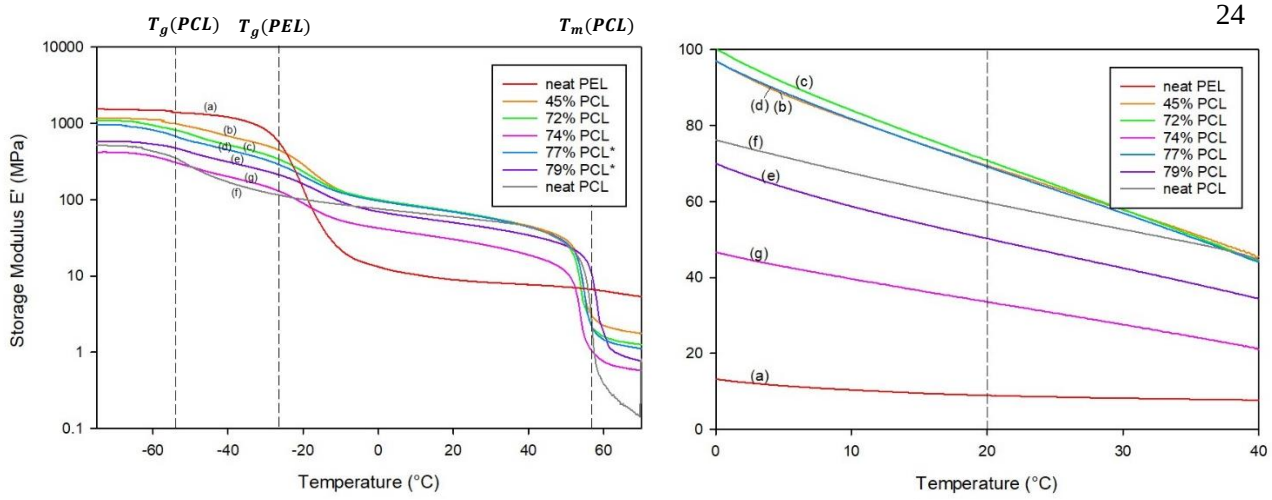

Figure 3-11: Comparison of storage modulus for PCL:PEL core-sheath fibers. Storage modulus near room temperature (20 ℃) is shown on the right.

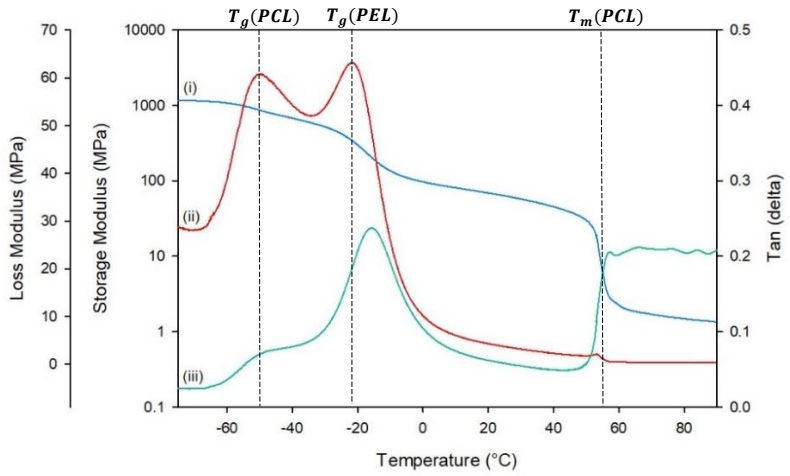

Figure 3-12: Representative DMA curves – i) storage modulus, ii) loss modulus, iii) tan delta- of 45% PCL:PEL core-sheath webs with visible T_g of PCL and PEL and T_m of PCL. Storage modulus is in logarithmic scale.

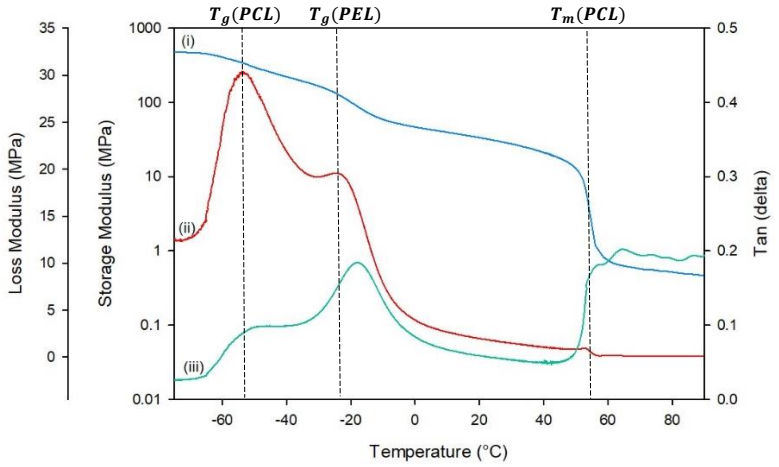

Figure 3-13: Representative DMA curves – i) storage modulus, ii) loss modulus, iii) tan delta- of 74% PCL:PEL core-sheath webs with visible T_g of PCL and PEL and T_m of PCL. Storage modulus is in logarithmic scale.

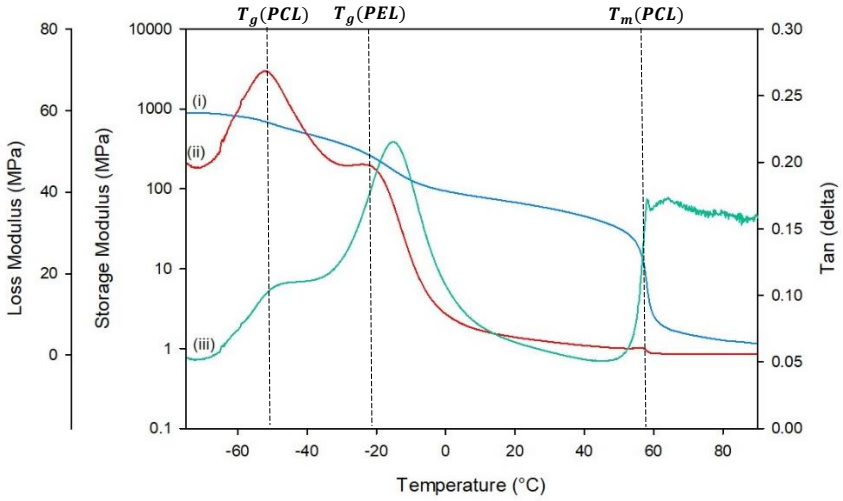

Figure 3-14: Representative DMA curves – i) storage modulus, ii) loss modulus, iii) tan delta- of 72% PCL:PEL core-sheath webs with visible T_g of PCL and PEL and T_m of PCL. Storage modulus is in logarithmic scale.

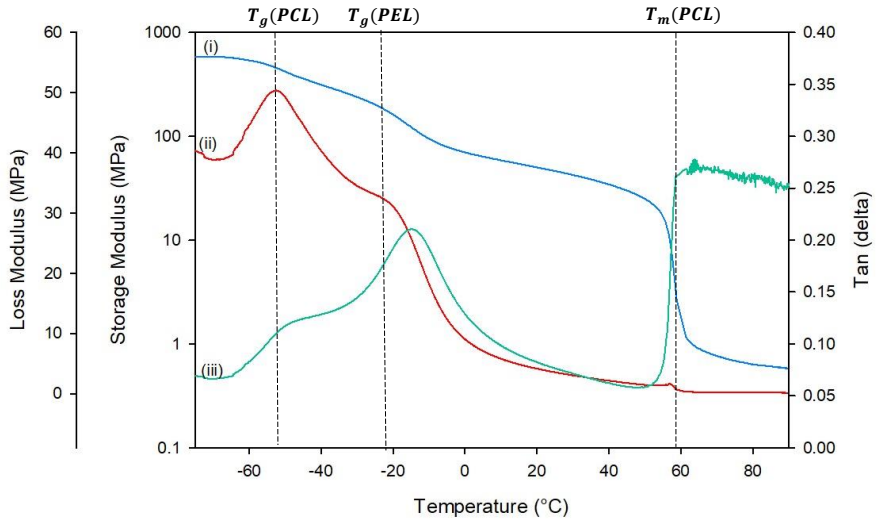

Figure 3-15: Representative DMA curves – i) storage modulus, ii) loss modulus, iii) tan delta- of 79% PCL:PEL* core-sheath webs with visible T_g of PCL and PEL and T_m of PCL. Storage modulus is in logarithmic scale

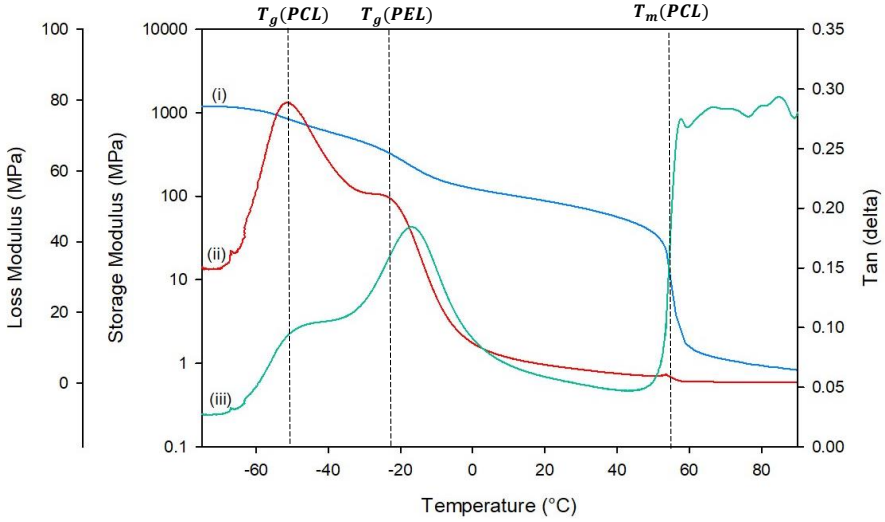

Figure 3-16: Representative DMA curves – i) storage modulus, ii) loss modulus, iii) tan delta- of 77% PCL:PEL* core-sheath webs with visible T_g of PCL and PEL and T_m of PCL. Storage modulus is in logarithmic scale.

3.5 Tensile Testing

Stress and strain-to-failure were evaluated for PCL:PEL core-sheath composites, and Young's modulus (MPa) was obtained from the slope of the linear elastic region. Figure 3-16 to 3-20 shows stress-strain curves (three trials) for each core-sheath composite. 45% PCL:PEL exhibited the highest strain at failure at 1300% (resembling that of neat PCL) while other core-sheath composites ranged between 600-800% strain with 7-8 MPa of stress at break. Young's modulus for core-sheath composites were closer to E for neat PCL at 18.087 ± 1.309. Stress and strain at break and young's modulus for each sample is summarized in Table 3-4.

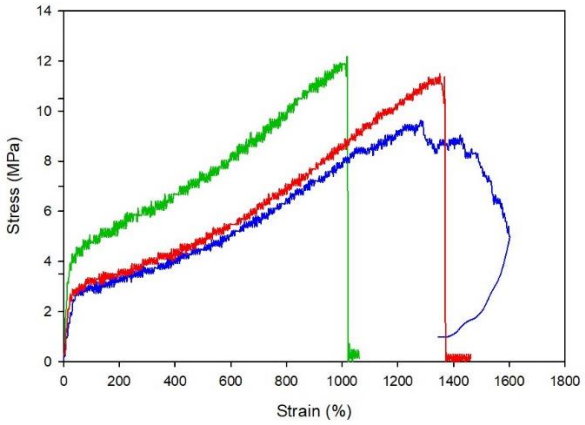

Figure 3-17: Stress-Strain curves for 45% PCL:PEL core-sheath composites measured until fracture for three trials.

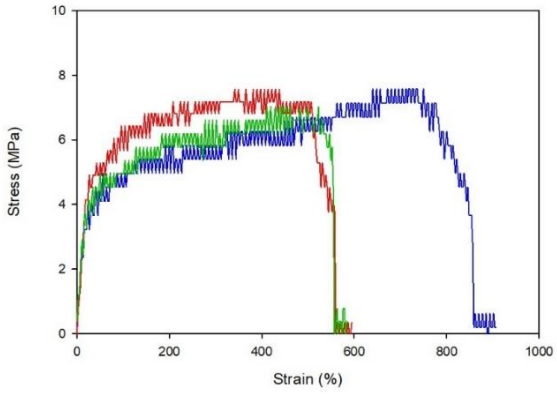

Figure 3-18: Stress-Strain curves for 74% PCL:PEL core-sheath composites measured until fracture for three trials.

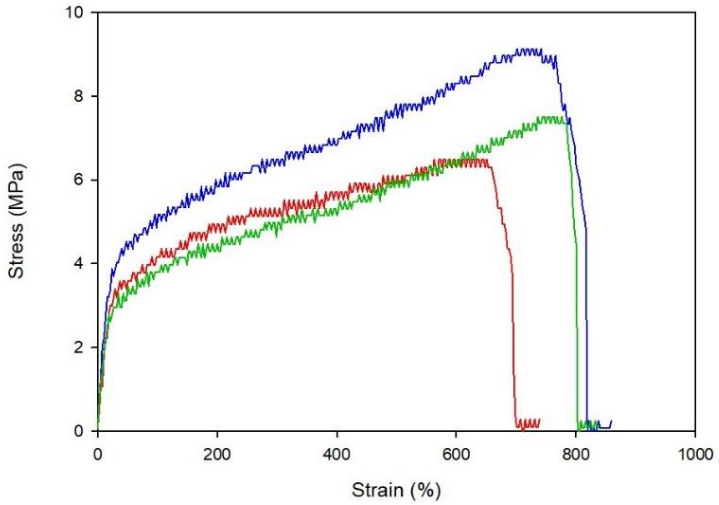

Figure 3-19: Stress-Strain curves for 72% PCL:PEL core-sheath composites measured until fracture for three trials.

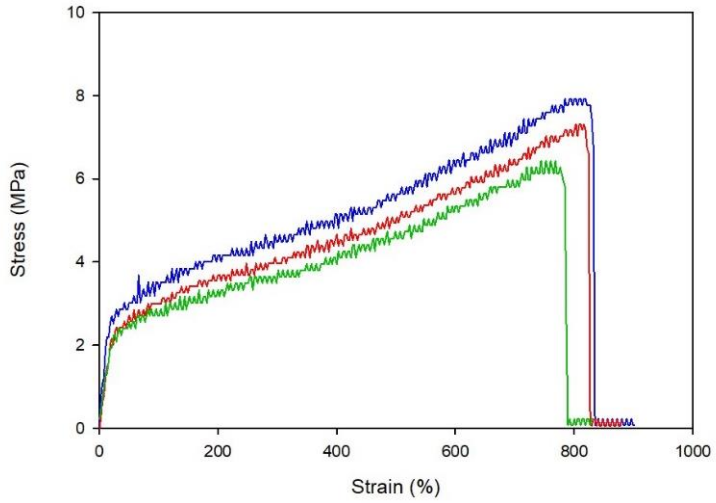

Figure 3-20: Stress-Strain curves for 79% PCL:PEL* core-sheath composites measured until fracture for three trials.

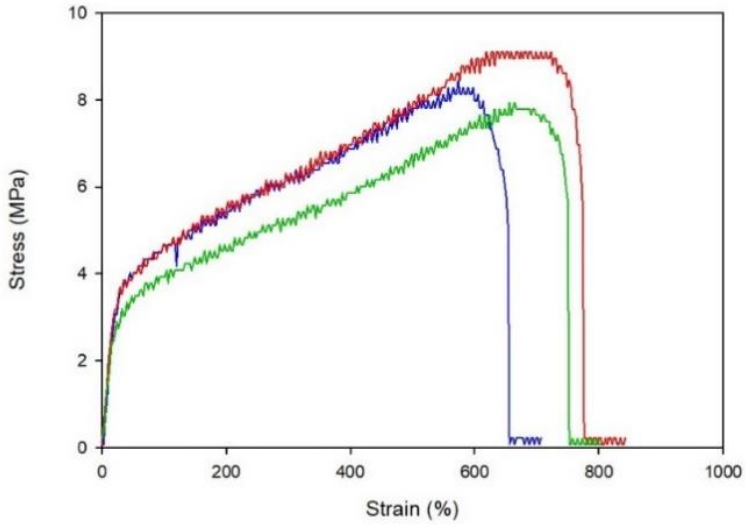

Figure 3-21: Stress-Strain curves for 77% PCL:PEL* core-sheath composites measured until fracture for three trials.

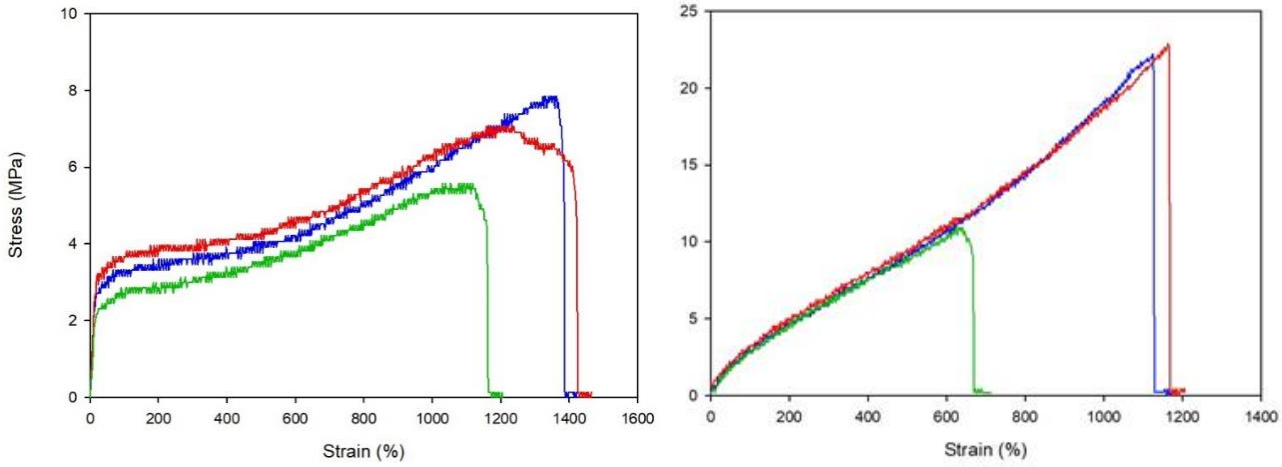

Figure 3-22: Stress-Strain curves for neat PCL (left) and neat Pellethane (right) measured until fracture for three trials.

Table 3-4: Stress (MPa) and Strain (%) at failure and Young's modulus for PCL:PEL core-sheath composites with varying PCL content.

Sample	Strain (%) @Break	Stress (MPa) @Break	E (MPa)
45% PCL:PEL	1282.46 ± 243.15	13.193 ± 2.294	13.383 ± 0.937
72% PCL:PEL	729.28 ± 66.58	7.483 ± 1.262	16.193 ± 1.128
74% PCL:PEL	594.98 ± 143.48	6.854 ± 0.268	17.295 ± 1.680
77% PCL:PEL*	611.87 ± 16.94	8.191 ± 0.726	14.627 ± 0.824
79% PCL:PEL*	800.43 ± 32.79	7.074 ± 0.748	10.813 ± 0.603
pure PCL	1270.01 ± 134.04	6.538 ± 1.127	18.087 ± 1.309
pure PEL	975.61 ± 295.67	18.509 ± 6.788	3.108 ± 1.088

3.5 Shape Memory

Shape memory curves for each PCL:PEL composite is shown in Figures 3-22 to 3-26. Table 3-5 shows the shape fixing and shape recovery ratios for PCL/PEL core-sheath composites over each shape memory program cycle, and shape fixing and shape recovery as a function of PCL composition. Samples were deformed with a programmed stress of 0.35 MPa. Good shape fixity was observed above 98% consistently for all samples and for each cycle. The shape recovery ratio increases over the course of each cycle with recovery ratios ranging from 70-90%.

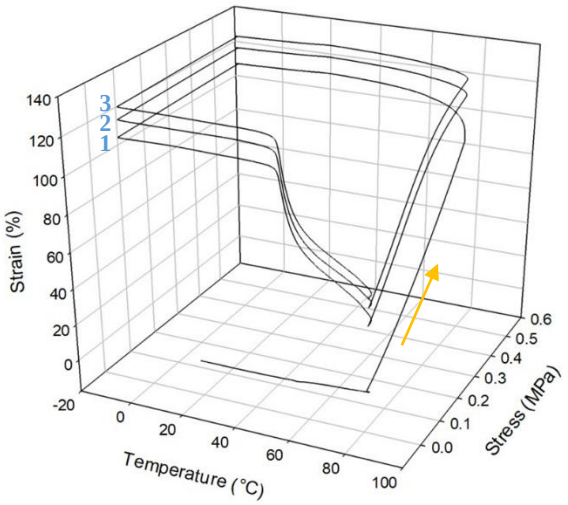

Figure 3-23: Three-loop one-way shape memory curve for 45% PCL of PCL/PEL core-sheath with strain as a function of temperature and stress at 0.5 MPa programmed stress.

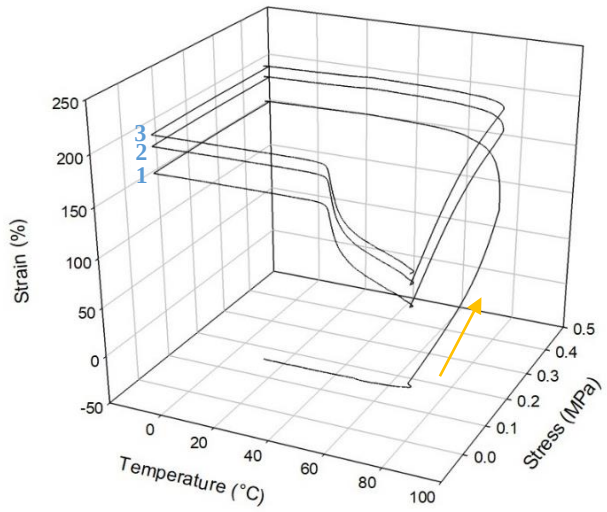

Figure 3-24: Three-loop one-way shape memory curve for 74% PCL of PCL/PEL core-sheath with strain as a function of temperature and stress at 0.35 MPa programmed stress.

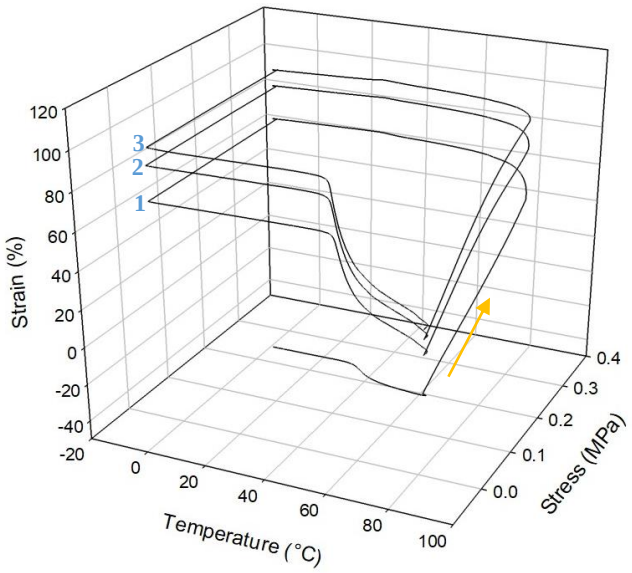

Figure 3-25: Representative three-loop one-way shape memory curve for 72% PCL of PCL:PEL core-sheath with strain as a function of temperature and stress at 0.35 MPa programmed stress.

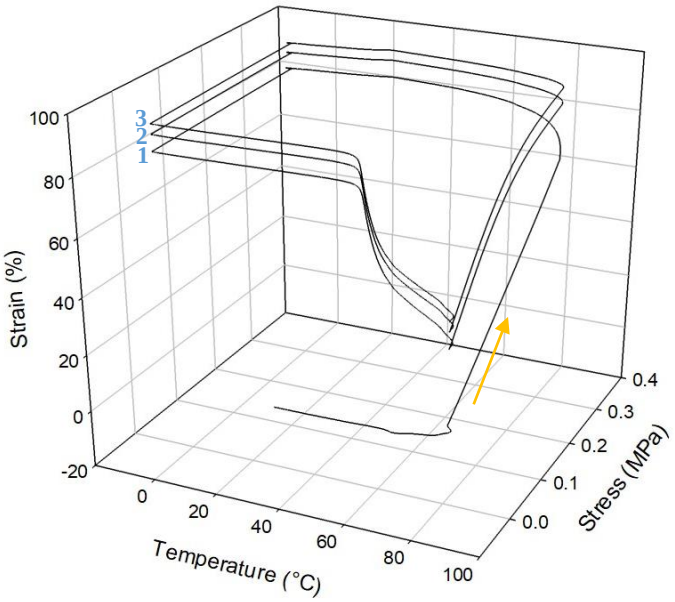

Figure 3-26: Representative three-loop one-way shape memory curve for 77% PCL:PEL* core-sheath with strain as a function of temperature and stress at 0.35 MPa programmed stress.

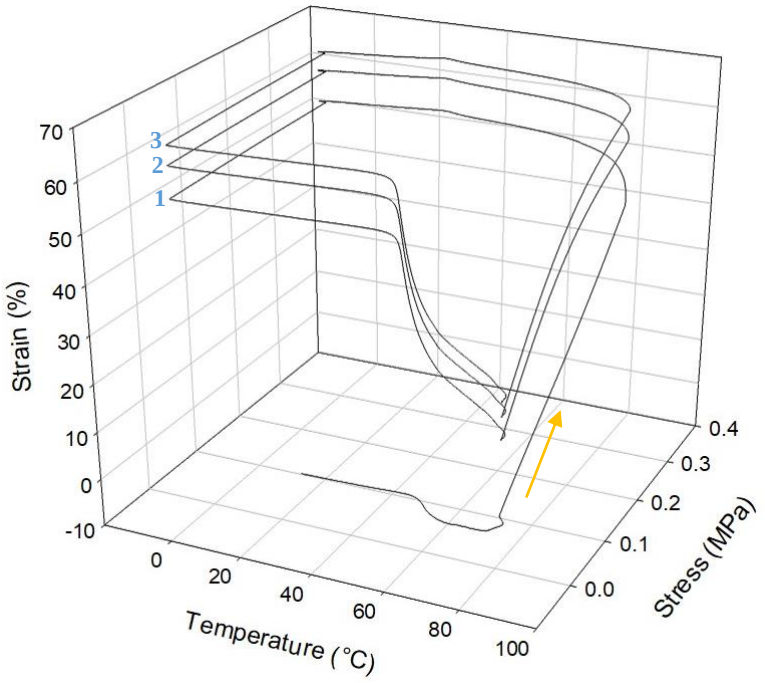

Figure 3-27: Representative three-loop one-way shape memory curve for 79% PCL:PEL* core-sheath with strain as a function of temperature and stress at 0.35 MPa programmed stress.

Table 3-5: Shape fixing and shape recovery ratios for each shape memory cycle for PCL:PEL composites with varying PCL content.

	Cycle 1		Cycle 2		Cycle 3	
Sample	**Rr (%)**	**Rf (%)**	**Rr (%)**	**Rf (%)**	**Rr (%)**	**Rf (%)**
45% PCL:PEL	70.41	98.35	87.75	97.98	93.72	97.97
74% PCL:PEL	52.62	99.20	80.71	98.66	89.10	98.43
72% PCL:PEL	64.38	98.80	83.55	97.95	93.27	99.03
79% PCL:PEL*	66.00	99.13	86.44	98.71	92.78	98.64
77% PCL:PEL*	69.75	99.04	88.52	98.61	93.54	98.58

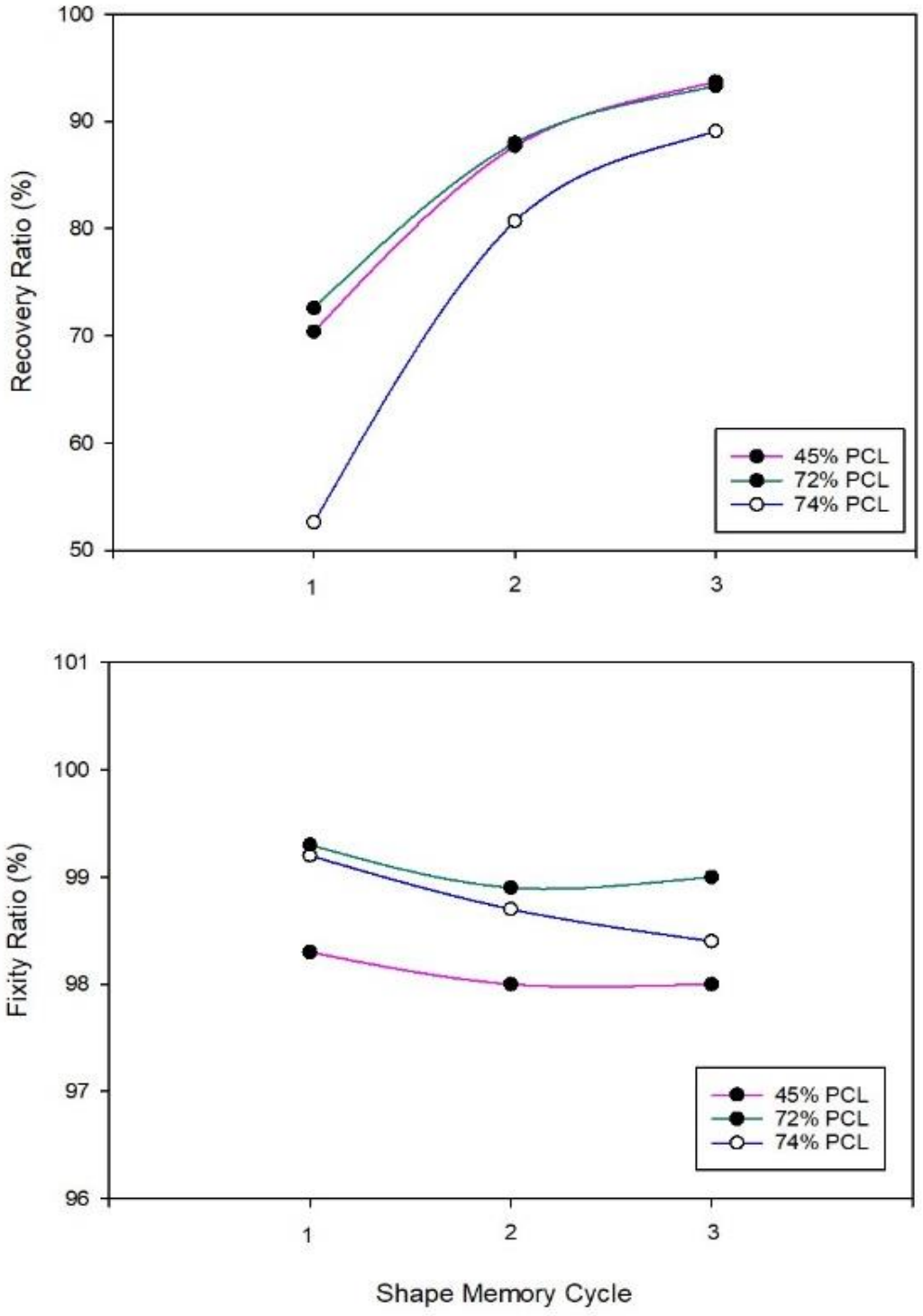

Figure 3-28: Progression of shape recovery (top) and shape fixity ratios (bottom) for three-cycle shape memory program at 0.25 MPa programmed stress.

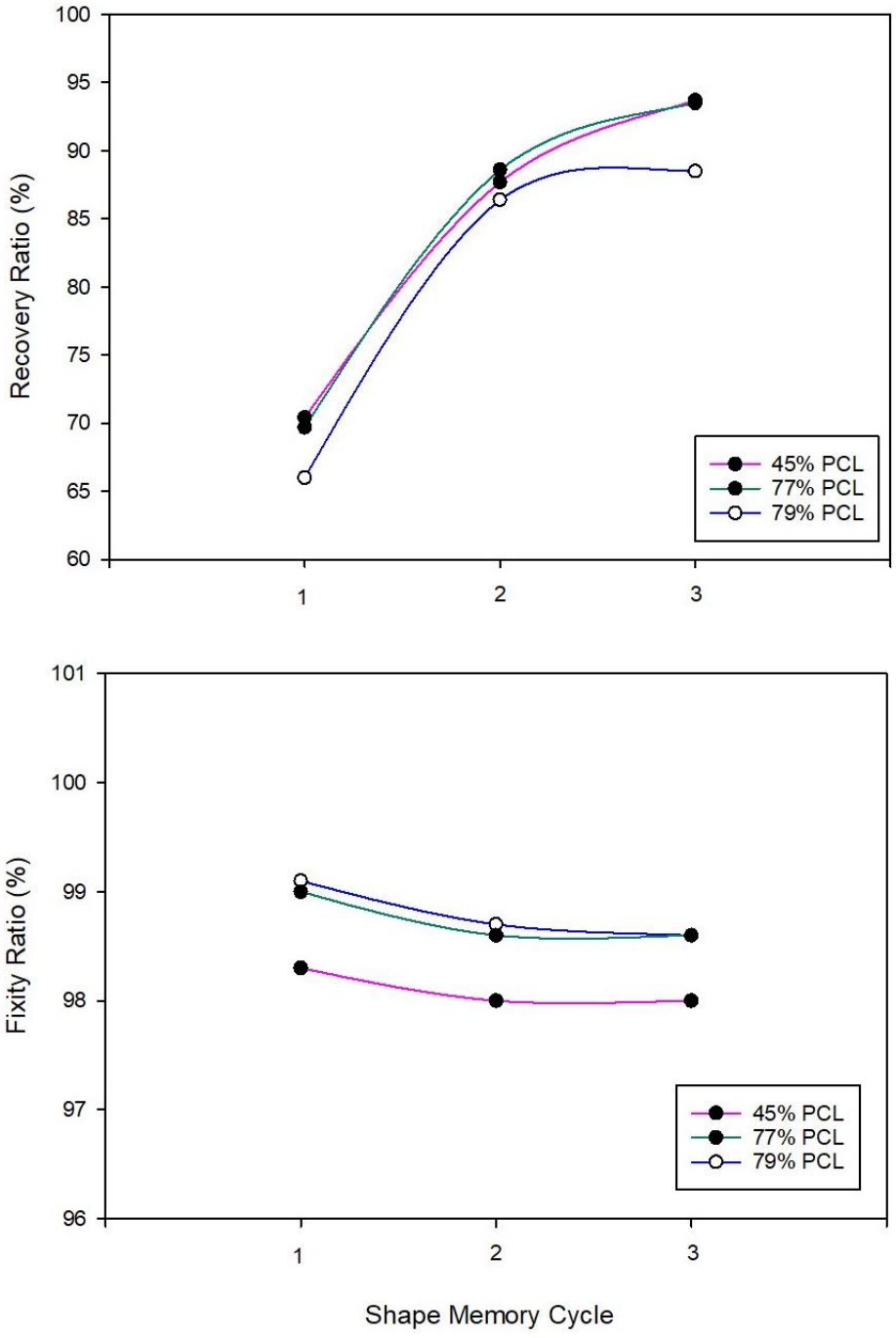

Figure 3-29: Progression of shape recovery (top) and shape fixity ratios (bottom) for three-cycle shape memory program at 0.35 MPa programmed stress (samples with controlled PEL core).

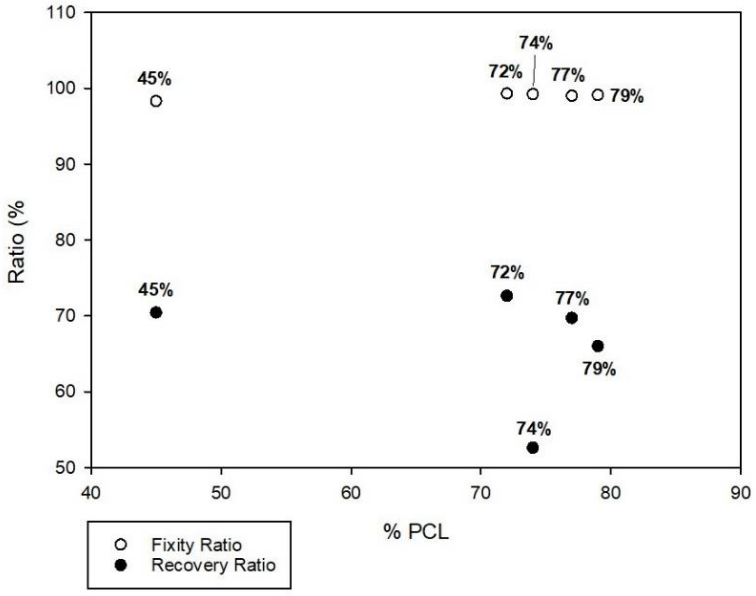

Figure 3-30: Shape Recovery and Shape Fixity ratios as a function of PCL composition for PCL/PEL for first shape memory cycle.

3.6 Discussion

In designing the core-sheath PCL:PEL webs, careful consideration was given to the critical range that existed for each electrospinning parameter (solution flow rates, applied voltage, etc.) within which coaxial electrospinning could operate for our materials. Therefore, to study the effect of changes in PCL composition on thermal and mechanical properties including shape memory in core-sheath composites, the flow rates of PCL and Pellethane were varied slightly to increase the amount of the Pellethane in the sample without disrupting the equilibrium required for this electrospinning technique. For a 10% and 25% increase in Pellethane, the flow rates of PCL and Pellethane for each sample varied by 0.2-0.7 mL/hr, resulting in composites containing 70-80% PCL. This limited range obscured observable trends in the properties for these materials occurring as a result of the change in composition.

The shape memory of PCL:PEL core-sheath composites maintained high shape fixing above 97% for all samples. Shape fixing - a measure of the deformation maintained after unloading the programmed stress – is strain energy stored by the crystallization of PCL. On the stress-temperature-strain curves, visually, a material with ideal shape fixing (R_f = 100%) is able to retain its temporary state and would not experience a decrease in strain after unloading. A negative slope of the curve in this region emphasizes unideal shape fixing. Thus, a slight increase in the shape fixing ability of the fibers was observed in composites with higher %PCL (compared to 45% PCL:PEL) as expected. This correlates with findings that dual-spun SMECs also exhibited higher shape fixing with increases in PCL content[5]. At 31% PCL composition, Robertson et. al reported a shape fixing ratio of approximately 90% compared to 40% shape fixing for 2% PCL[5].

Regarding shape recovery for PCL:PEL core-sheath composites, R_r averaged around 64% for the first shape memory cycle, 85% for the second loop, and 92% for the third for all core-sheath webs. Figure 3-27 and 3-28 show that percent shape recovery increases significantly before leveling off after the first and second shape memory cycle (deformation, fixing, recovery). Because fibers were not compressed to a film prior to shape memory testing, heating from the first cycle melded PCL fibers together for stronger chain interactions, likely forming a matrix around intact Pellethane fibers in the web. While this does not provide insights on the reliability of shape memory performance over time, it can be expected that shape recovery around 90% can be achieved after film compression. Furthermore, given that shape recovery relies on Pellethane's elasticity, changes in PCL composition did not alter shape recovery ratios. Robertson et. al reported similar results for dual spun PCL:PEL SMEC films with recovery ratios above 90% and no variation among samples with different PCL content[5].

In addition to high shape fixity and shape recovery, these materials also exhibited reversible adhesive properties. When heated above PCL's melting temperature, the core-sheath webs acted as strong adhesives when cooled to allow crystallization of PCL. While beyond the scope of this thesis, investigation of this phenomenon is recommended.

Chapter 4

Conclusion & Future Work

A novel core-sheath polymer composite of PCL and Pellethane was fabricated using coaxial electrospinning techniques and characterized with demonstrated shape memory behavior and reversible adhesive properties. Insights and limitations of coaxial electrospinning were noted, prompting a need to improve control over fiber properties while balancing the delicate conditions required. The critical ranges for electrospinning parameters such as applied voltage, flow rates, and solution viscosity for these core-sheath components require further research, enabling control over fiber composition. Future work should also explore the use of these materials for drug delivery systems, identifying compatible drugs to load within the core and sheath layers, as well as detailed investigation of the reversible adhesive properties.

BIBLIOGRAPHY

(1) Bonk, H. W.; Sardanopoli, A. A.; Ulrich, H.; Sayigh, A. A. R. Pellethane®: A New Generation of Polyurethane Thermoplastic Elastomers. *Journal of Elastoplastics* **1971**, *3* (3), 157–186. https://doi.org/10.1177/009524437100300302.

(2) Qin, X. Coaxial Electrospinning of Nanofibers. *Electrospun Nanofibers* **2017**, 41–71. https://doi.org/10.1016/B978-0-08-100907-9.00003-9.

(3) Moghe, A. K.; Gupta, B. S. Co-axial Electrospinning for Nanofiber Structures: Preparation and Applications. *Polymer Reviews* **2008**, *48* (2), 353–377. https://doi.org/10.1080/15583720802022257.

(4) Díaz, J. E.; Fernández-Nieves, A.; Barrero, A.; Márquez, M.; Loscertales, I. G. Fabrication of Structured Micro and Nanofibers by Coaxial Electrospinning. *J Phys Conf Ser* **2008**, *127*, 012008. https://doi.org/10.1088/1742-6596/127/1/012008.

(5) Robertson, J. M.; Birjandi Nejad, H.; Mather, P. T. Dual-Spun Shape Memory Elastomeric Composites. *ACS Macro Lett* **2015**, *4* (4). https://doi.org/10.1021/acsmacrolett.5b00106.

ACADEMIC VITA

Asna Rizwan
atr5249@psu.edu

EDUCATION

The Pennsylvania State University, Schreyer Honors College **University Park, PA**
Eberly College of Science | Major: B.S Chemistry *Class of May 2023*
Activities: Alpha Omicron Pi, Nittany Chemical Society, Schreyer for Women, Remote Area Medical, Mock Trial, UPUA, Panhellenic Council

RELEVANT EXPERIENCE

Mather Research Group **University Park, PA**
Undergraduate Research Assistant | Department of Chemical Engineering *April 2022 - Current*
- Fulfilling the thesis requirement for the Schreyer Honors College under the supervision of Dr. Patrick T. Mather
- Investigate morphology of Pellethane® and poly(ε-caprolactone) nanofiber composites and shape memory properties
- Mentor and train incoming students on polymer fabrication and material characterization techniques

CHEM 210 Organic Chemistry **University Park, PA**
Learning Assistant, Dr. Joseph Houck | Eberly College of Science *August 2021 - Current*
- Provide classroom assistance to a approximately 300 undergraduates to develop fundamental organic concepts
- Devise individual learning plans for students/monitor student progress during weekly hosted office hours & workshops
- Communicate student feedback; discuss upcoming curriculum and learning strategies with instructor during weekly meetings

The Monshausen Lab **University Park, PA**
Undergraduate Research Assistant | Department of Biology *Dec 2019 – May 2020*
- Research FER-dependent mechanical and RALF signaling under Dr. Gabriele Monshausen
- Communicated weekly findings with PI and graduate students; discussed plan for upcoming week
- Assisted in data collection and analysis according to research protocols, employing sterile technique, adhere to lab safety standards
- Assist with sample preparation, instrument setup, and essential laboratory upkeep

VOLUNTEER & LEADERSHIP EXPERIENCE

Alpha Omicron Pi **University Park, PA**
Overall Recruitment Team; Director of Panhellenic Relations | Epsilon Alpha Chapter *Dec 2021 - Current*
- Facilitate communication between chapter Executive Team and AOII Headquarters and collaborate with larger Greek community
- Propose initiatives to uphold chapter values and promote diversity and inclusion within Greek Life
- Coordinate recruitment in accordance with NPC guidelines for 17 Panhellenic chapters and approximately 1600 potential new members

Presidential Leadership Academy **University Park, PA**
Senior Class | Schreyer Honors College *Apr 2020 - Current*
- Selected as one of 30 freshmen to participate in 3-year Presidential Leadership Academy Certificate Program
- Engage in courses taught by Penn State President Dr. Eric Barron, and Schreyer Honors College Dean, Patrick Mather
- Develop critical thinking, policy-making and leadership skills, and tackle civic issues in society and university administration

Student Conduct Advisors **University Park, PA**

Student Conduct Advisor | University Park Undergraduate Association *December 2019 – December 2021*

- Provide non-legal advice to students who may have violated any university policy
- Guide students through the Conduct process and attend Conduct Conversations/hearings to provide support to students

HONORS & COURSEWORK

- **Honors:** Albert Welford Castleman, Jr. Memorial Scholarship, Fleming-Meyer Analytical Chemistry Award, K. Elizabeth Howe Memorial Scholarship, Schreyer Academic Excellence Scholarship, Provost's Award, Dean's List, Lisa M. Waller Striving for Excellence
- **Courses:** Analytical Chemistry, Chemistry Professional Development, Honors Chemical Principles I & II, Organic Chemistry I & II, Experimental Organic Chemistry, Biology of Molecules & Cells, Honors Biochemistry I, Critical Thinking & Leadership
- **Skills:** Dynamic Mechanical Analysis, Differential Scanning Calorimetry, Scanning Electron Microscopy, Electrospinning, Polymer Fabrication, Sample Preparation, Chromatography, Spectroscopy, Gel Electrophoresis, DNA Extraction, Organic Synthesis, Sterile Technique, Literature Review, Microsoft Office